Normalized Cumulative Periodogram Method For Tuning A Regularization Parameter of The EEG Inverse Problem

Mohammed J. Aburidi * • Adnan Salman

Computer Science Department, An-Najah National University, P.O. Box: 7, Nablus, Palestine
mohammed.ridi114@gmail.com

Abstract: Investigation of the functional neuronal activity in the human brain depends on the localization of Electroencephalographic (EEG) signals to their cortex sources, which requires solving the source localization inverse problem. The problem is ill-conditioned and under-determinate, and so it is ill-posed. To find a treatment of the ill-posed nature of the problem, a regularization scheme must be applied. A crucial issue in the application of any regularization scheme, in any domain, is the optimal selection of the regularization parameter. The selected regularization parameter has to find an optimal tradeoff between the data fitting term and the amount of regularization. Several methods exist for finding an optimal estimate of the regularization parameter of the ill-posed problems in general. In this paper, authors investigate the normalized cumulative periodogram (NCP) and apply it to the source localization problem. Furthermore, authors compare its performance with other two parameter choice methods which are L-curve and Generalized-Cross Validation (GCV) in terms of accuracy and reliability. Authors opted the WMNE algorithm to solve the EEG inverse problem with the application of different noise levels and different simulated source generators. Our results indicate that NCP method gives the best estimation for the regularization parameter in general. However, for some levels of noise, GCV method has similar performance. In contrast, both NCP and GCV methods outperform the L-curve method and resulted in a better average localization error.

1. Introduction:

In neuroscience, the accuracy of brain imaging techniques like electroencephalography (EEG) (Grech et al., 2008; Tucker, 1993) and magnetoencephalography (MEG) (Van Uitert et al., 2003), requires solving what is called the *source localization problem*. The source localization problem is the problem of inferring an estimate of the brain current sources that generate the electric potentials on the scalp and the magnetic field near the scalp. These fields are measured using recording sensors technologies (Tucker, 1993).

Electromagnetic-based (EM) imaging techniques like EEG and MEG provide a direct measurement of the neural activity in the range of milliseconds temporal resolution (Modarreszadeh & Schmidt, 1997). However, due to the ill-posed nature of the neuroscience source localization problem and the volume conduction characteristics of the human head (Greenblatt et al., 2005; Pascual-Marqui, 1999; Pascual-Marqui, 2002), the spatial resolution is limited to few centimeter. In contrast, indirect imaging modalities such as functional Magnetic Resonance Imaging (fMRI) (Liu et al., 1998) and Positron Imaging Tomography (PET) (Cherry, & Phelps, 1996), provide indirect measurements of brain spatiotemporal activity in the range of seconds temporal resolution and millimeter spatial resolution. Therefore, improving the spatial resolution of EM-based imaging will allow achieving a high spatiotemporal brain functional imaging.

Two approaches are used in solving the source localization problem (Grech, et al., 2008) the equivalent dipole model (Tucker, 1993), and the distributed dipole model (Grech, et al., 2008; Darvas et al., 2004; Baillet et al., 2001). The equivalent dipole model is based on the assumption that the scalp EEG signal is generated by one or few current dipoles, whose locations and moments to be determined using a nonlinear search algorithm (Fender, 1987; Scherg, & Von Cramon, 1985). The drawback of this approach is the required specification of the number of dipoles. Underestimating them causes biased results by the missing dipoles. Overestimating them, causes the dipoles to fit any data. In the distributed model approach, the primary current sources are assumed to be current dipoles

distributed inside the brain. The number of dipoles must be large enough (~10,000) to cover the cortex with an optimal resolution. Then, the potentials due to these dipoles at the scalp electrodes is computed using the forward solver of Poisson equation to obtain a *lead field matrix* (LFM), which provides the linear relationship between the current dipoles and potentials at the scalp electrodes, $\Phi = K J + \epsilon$ (Tong, & Thakor, 2009). Then, the goal of the source localization problem is to solve the forward equation to find an estimate of the current sources J, given the LFM K and a scalp measurements Φ_{EEG}.

However, since the LFM K is 1) ill-condition (has high condition number), causes unstable highly-sensitive solutions to noise and 2) underdetermined, the number of dipoles (columns) is much higher than the number of electrodes (rows), which means the solution is not unique and there are an infinitely many solutions that would explain a given EEG signal. One approach to find a unique and stable solution is to apply a regularization scheme (Pascual-Marqui, 1999; Pascual-Marqui, 2002).

In this approach, the inverse solution is approximated by a family of stable solutions. However, these regularization schemes involve a *regularization parameter* α that controls a tradeoff between the stability of the solution and the goodness of the fit to the data. Overestimating *α*, results in a stable solution but bad fit to the data. Underestimating α, cause a good fit to the data, but the unstable solution. Therefore, tuning and finding the optimal value of α is crucial to the quality of the solutions. In the literature, there exist several methods for tuning the regularization parameter includes: L-curve (Hansen, & O'Leary, 1993; Hansen, 1994), normalized cumulative periodogram (NCP) (Hansen, et al., 2006; Hansen, & Kilmer, 2007), and the Generalized-cross validation (GCV)(Wahba, 1977; Golub et al., 1979).

However, the quality of each method likely depends on the characteristic of the particular inverse problem. In this paper, authors investigated the quality of these methods in tuning the regularization parameter for neuroscience source localization problem. Authors compared their performance and the quality of the inverse solution using three measures of error, localization error (Pascual-Marqui, 2002), the center of gravity (Baillet, 1998; Salman et al., 2013), and spatial spreading (Pascual-Marqui, 1999). Authors solved the inverse problem using WMNE algorithm (Hamalainen, 1984; Lin et al., 2006).

2. Background concepts:

2.1. Forward Problem

In response to external stimuli, thousands or tens of thousands of arranged neurons are activated in a way that their induced current adds up. This net current is strong enough to propagate through the head tissues to the scalp where it can be measured using EEG sensors. These current generators are well accepted to be modeled as current dipole sources because the measuring sensors are far away

from the current source region. Computing the electric potential on the scalp for a given current dipole source inside a brain is a well-defined problem, called the EEG forward problem (Rubio, & Troparevsky, 2006; Neilson et al., 2005). Formally, it can be stated as follows: Given a volume conductor with boundary Ω, current sources within the volume induce electric and magnetic fields which can be calculated on the surface. If the conductivities σ and the current sources S are known, the electric and magnetic fields inside the volume are fully described by the quasi-static approximation of Maxwell's equations–Poisson equation (Hämäläinen et al., 1993),

$$\nabla \cdot (\sigma \nabla \Phi) = S , \qquad (1)$$

where σ is the conductivity tensor, Φ is the potential, S is the current source. The solution of Equation depends on the volume conduction properties, geometry (Munck, & Peters, 1993; De Munck, 1988; Van Uitert, & Johnson, 2002) and conductivity (Clerc, et al., 2005; Oostendorp, et al., 2000; Gonçalves, et al., 2003; Meijs et al., 1988) and its solution can be obtained using numerical methods such as Finite Difference Method (FDM) and Finite Element Method (FEM). In this study, authors used an FDM solver that authors already have (Salman et al., 2013; Hallez et al., 2005).

2.2. Inverse Problem:

Several approaches are used to solve the source localization inverse problem (Darvas et al., 2004; Baillet, et al., 2001; Pascual-Marqui, 1999). However, in this study, authors only consider models based on the distributed dipole approach. In this approach, the brain is covered with a large number of dipoles N (N 5,000-10,000). Then the electrical potential due to each dipole at the scalp electrodes, called the lead field (the potential at M 32-512 scalp electrodes) is computed using the forward solver for the three orthogonal orientations of the dipole moment, *x, y,* and *z*. The lead field matrix defines the relationship between the dipole current density J and the electric potentials at the scalp electrodes Φ, in what is called, the forward linear equation,

$$\Phi = K J + \epsilon, \qquad (2)$$

where $K \in \mathrm{R}^{M \times 3N}$ is the Lead Field matrix with three donates for each current dipole, each element in K represents the electric potential due to its current source, $J \in \mathrm{R}^{3N \times 1}$ is the primary current density vectors, z is a perturbation error, and $\Phi \in \mathrm{R}^{M \times 1}$ is a vector containing scalp electric potentials measured at M sensors. Every row in K is a lead field corresponding to a current dipole obtained by solving the forward problem.

The goal of the inverse problem is to invert Equation 2 to find an estimate of the current densities column vector $\hat{J}$. Two issues must be addressed in finding a useful solution for the inverse problem:
1. The system is underdetermined since the number of unknowns (the locations and orientations of the distributed dipoles are in the range of thousands) is significantly larger

than the number of constraints (the number of electrodes in the range of hundreds).

2. The system is ill-conditioned since a small perturbation in the right-hand side Φ_{EEG} due to noise or a small perturbation to the coefficient matrix K would result in a large change in the solution.

To address these issues, a regularization term is added in order to give a preference to a particular solution with some desirable properties (Pascual-Marqui, 1999; Pascual-Marqui, 2002), and also to improve the conditioning of the problem and obtain a unique and stable solution. Then instead of minimizing the sum of the squared residuals only, a regularization term is added, and the problem becomes to minimize,

$$F_\alpha(J) = \|\Phi_{EEG} - K\,J\|^2 + \alpha\|\Gamma J\|^2, \qquad (3)$$

Where $\|\Gamma J\|^2$ is the constraints and regularization term, $\|K\,J - \Phi_{EEG}\|$ is the data fitting term or residual norm, and α is the regularization parameter. The regularization parameter α must find a good compromise between the two norms in order to minimize the error in the regularized solution. Overestimating α results in a stable solution but a bad fit to the data. Underestimating α, causes a good fit to the data, but the unstable solution.

3. Methods and Materials:

Modeling the Human Head:

Solving the source localization problem using the distributed dipole model approach require first solving the forward problem that maps a current source generator inside the brain to the scalp potentials at the electrodes. The forward problem is a well-posed problem that has a unique solution. To solve the forward problem, first, authors need to build a computational head model. In this model, the human head is modeled as a volume conductor consists of 5 different uniform tissues. The computational model requires a geometry model of the different tissues of the human head, and a conductivity model to assign a conductivity for each tissue.

The geometry model:

The geometry model defines the boundaries between different tissues of the human head. Medical imaging such as Magnetic Resonance Imaging (MRI) provides images of anatomical details with resolution better than 1 $mm3$. These images can be segmented to a number of tissues where each tissue is assumed to have uniform electrical properties. In this study, authors used the geometrical model obtained from an MRI image with a resolution of 1 $mm3$ for a subject, segmented into five uniform tissues, white matter, gray matter, CSF, skull, and scalp. Figure 1 shows these tissues. The segmented image is obtained from previous work done at Neuroinformatic Center (University of Oregon) and Electrical Geodesics Incorporated (EGI).

(a) Scalp   (b) White matter

(c) Skull   (d) Gray matter
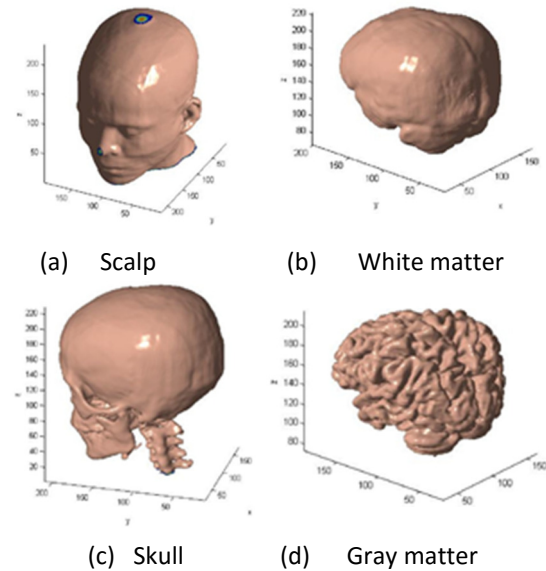
Figure 1. Geometric model of the tissues of the human head.

The conductivity model:

Once different tissues of the human head are identified from the segmented MRI image, a conductivity model and values must be specified. In this study, authors assumed the conductivities of all tissues are isotropic and have values obtained from the literature and shown in Table 1.

Table 1: *Tissues Parameters in realistic head model*

Tissue Type	$\sigma(\Omega^{-1}m-1)$	Reference
Gray matter	0.25	Geddes (1967)
Csf	1.79	Daumann (1997)
Scull	0.0180	Law (1993)
Scalp	0.44	Burger (1943)
White matter	0.35	Ferree(2000)

The forward solver algorithm:

In this study, authors used the Alternating Direction Implicit (ADI) method, which is a finite difference method FDM to solve Poisson equation. The solver was implemented in previous work (Salman et al., 2013). The solver is efficient and can handle only isotropic tissues. Using the forward solver, authors can calculate the potential of the scalp electrodes for a given current source modeled as a current dipole inside the brain.

The current source model:

It is well accepted to model a current source generator inside the brain as a current dipole consists of a current source and a current sink placed close to each other. To obtain the potential due to a current dipole source with arbitrary orientation, authors first computed the potential due to three orthogonal unit dipoles placed along the x, y

and z-axis to obtain their potentials, $\varphi_x, \varphi_y,$ and φ_z, respectively, at the scalp electrodes, see figure 2. Then, since Poisson equation is linear regarding current sources, the potential corresponding to a dipole placed at the three orthogonal dipoles location with arbitrary orientation, given by the direction cosines (α, β, and γ) can be calculated by the superposition principle:

$$\Phi_{EEG} = \alpha\varphi_x + \beta\varphi_y + \gamma\varphi_z. \quad (4)$$
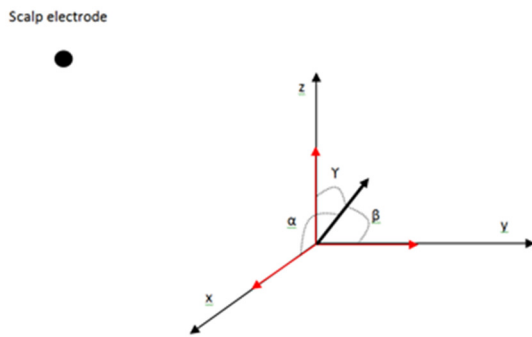
Figure 2. The potential corresponding to a dipole with arbitrary orientation is a linear combination of the potential due to three orthogonal unit dipoles.

The generics LFM (gLFM):

The generic Lead Field Matrix (gLFM) construct introduced in (Salman et al., 2013) serves as generators of LFMs. It maps the orthogonal generic dipole sources to generic electrodes potentials. Three orthogonal generic distributed dipoles are placed at every voxel in the gray matter and the generic electrodes are placed at 1 *mm*3 inter-spacings on the scalp.

Once a gLFM is computed using the forward solver, many different LFMs can be sampled based on different constraints or resolution imposed on the sources (*e.g.*, the number and locations of the electrodes). This can be achieved efficiently by sampling from the rows and columns of the gLFM appropriately. The computation of a gLFM factor out the common and computationally intensive part of the analysis from the application of different inverse algorithms.

In the case of distributed dipole models, the appropriate columns corresponding to imposing constraints on the sources are sampled as well. Then different distributed dipoles algorithms can be applied. In this study, authors used a gLFM matrix that was computed previously at University of Oregon computing cluster. Each row contains the potential due to three orthogonal dipole moments placed at every dipole location at a scalp electrode. And, every three column correspond to the potential due to three orthogonal dipoles at all electrodes.

Sampling the Lead field Matrix:

Different LFMs with differently distributed dipoles configuration and different scalp electrodes configuration can be downsampled from the gLFM. This is achieved by downsampling from the rows and columns of the gLFM. In this study, authors selected 128-electrodes uniformly distributed on the scalp from the generic electrodes and authors sampled 2500 current dipoles from the generic distributed dipoles, using the method illustrated in (Salman et al., 2013) at a resolution of 7 *mm.*

3.1. EEG Simulated data (Synthetic Data)

To test the accuracy of the inverse solution using different automatic regularization parameter tuning methods, authors simulated the EEG data corresponding to a current dipole source placed at the certain location and have a certain orientation following the simulation method in (Pascual-Marqui, 2007):
1. From the generic dipoles set, authors selected a dipole in a certain location *D*.
2. The potentials $\varphi_x, \varphi_y, \varphi_z$ due to the three orthogonal dipoles d_x, d_y, d_z in that location at the electrodes are then extracted from the gLFM.
3. For a certain dipole moment orientation (α, β, γ), authors calculated the potential to obtain the simulated EEG potential using equation 4.
4. A white Gaussian noise with different levels is added to Φ_{EEG}, to simulate noisy data. Authors used the Matlab function awgn() to generate the white Gaussian noise. This new generated potential vector represents the EEG potentials $\Phi_{EEG} \in R^{M \times 1}$.

3.2. Regularization parameter choice methods

A crucial issue in the application of any regularization scheme, in any domain, is the optimal selection of the regularization parameter. The regularization parameter controls the smoothness of the solution and tuning of this parameter is essential in achieving a meaningful and reliable solution. Several methods have been developed to automatically tune it (Hansen, & O'Leary, 1993; Hansen, 2001; Morozov, 1966; Krawczyk-StańDo, & Rudnicki, 2007; Wahba, 1977; Hansen, et al., 2006). In this study, authors estimate the regularization parameter using three methods, L-curve method, generalized cross-validation (GCV) and normalized cumulative peirdogram (NCP).

The L-curve method has emerged as a popular method over the past few years (Hansen, 1994). It considers a log-log plot of the regularized norm of the inverse solution versus the residual norm. The L-curve method produces a sharp corner shaped like 'L'. The optimal value of α corresponds to the corner of the curve since this point corresponds to a compromise between the two quantities. The corner of the curve can be computed by finding the maximum curvature of the curve κ (Hansen, 2001).

In GCV method, it has the following basic idea: the good value of regularization parameter should make K Jα able to predict the missing value on the right-hand side (Φexact in our case). Thus, the optimal value of α corresponds to the minimum value of the GCV function G(α) (Golub et al., 1979). The GCV function is given by,

$$G(\alpha) \quad \frac{\|KJ - \Phi_{EEG}\|^2}{(T_r(I - KK^{\S}))^2} \qquad (5)$$

3.2.1. The normalized cumulative periodogram (NCP)

This technique seeks to extract more statistical information available in the residual vector, which contains information that is worth extracting. The idea is to choose the largest regularization parameter that makes the residual vector resemble white noise vector (Hansen, & Kilmer, 2007). Authors start to choose a large α and reduce it until having a residual vector that looks like white noise vector in terms of the frequencies of the power spectrum of the residual vector. It uses Fourier Transform to change the time domain of the residual vector to be in the frequency domain in order to compute its normalized cumulative periodograms $C(r_\alpha)$.

The definition of the NCP for the Tikhonov residual vector can be as the vector $C(r_\alpha)$ whose elements involve the cumulated sums of the power spectrum:

$$C(r_\alpha)_I = \frac{p(\alpha)_2 + ... + p(\alpha)_{i+1}}{p(\alpha)_2 + ... + p(\alpha)_{q+1}} . \qquad (6)$$

where $P(\alpha)$ is the power spectrum (peridogram) of the residual vector can be obtained by using Discrete Fourier transforms. The optimum alpha for NCP is the corresponding to the minimum value of the function D:

$$D(\alpha) = \|C(r_\alpha) - C_{white}\|_2 \qquad (7)$$

The Matlab regularization toolbox (Hansen, 1994) was used to compute the parameter and apply regularization technique.

3.3. Discrete Picard Condition:

An important condition must be satisfied to apply L-curve and NCP method for tuning the regularization parameter. This condition is called the Discrete Picard Condition which states that the decaying of Fourier coefficients on an average, must be faster than the decay of the singular values of the lead field matrix. Because of the presence of the noise, authors don't expect to, Therefore, investigating Picard condition is necessary to find out whether a useful solution can be obtained. If the Picard Condition is not satisfied, there is no reason to solve the ill-posed problem. To do this, authors made the plots of the discrete Picard for the simulated EEG potential concerning all the three locations of the current dipoles (Superficial, at the middle and deeply located dipoles).

3.4. Tuning the regularization parameter α and solving the Inverse Problem

For this study, authors selected several EEG data sets as described above corresponding to three locations inside the brain. One location is superficial (D1), which is close to the surface of the brain. The second location is in the middle region of the brain, at about the middle distance between the center of the brain and the surface of the brain (D2). The third location is deep inside the brain close to the center (D3). The reason for these choices is to include into consideration the fact that the minimum norm estimate inverse problem solver is biased toward superficial sources. For each dipole location, authors considered 30 different orientations selected by uniformly distributing 30 points on a unit sphere centered at each dipole location. For each dipole location and orientation, authors considered 128 electrodes uniformly distributed on the scalp. Then, authors used distributed dipole grid spacing of 7 *mm* to localize each dipole location and orientation.

3.5. Error Evaluation Measures:

Authors considered three error measures to evaluate the influence of the number of scalp sensors N_e and solution space resolution on the source localization accuracy. The first measure is the Localization error (Pascual-Marqui, 2002). It was defined as the distance between the actual test source and the location of the maximum estimated current. The second measure is the spatial spreading or blurring of the solution (Pascual-Marqui et al.,1999). It corresponds to a measure of the spatial standard deviation of the imaging method centered at the actual test sources. Defined as:

$$Spreading = \sqrt{\frac{\sum_{i=1}^{M} \|r_i - r_{test}\|^2 \|J_i\|}{\sum_{i=1}^{M} \|J_i\|^2}}, \qquad (8)$$

Where r_{test} is the actual test dipole location, r_i is the location of the ith source, and j_i is the estimate of the current density.

The final measure that authors sued is the Euclidean distance between the actual dipole location and the center of gravity (COG) of WMNE source estimate scores, defined as (Salman et al., 2013; Baillet, 1998):

$$COG = \left| \frac{\sum_{i=1}^{M} \|J_i\| \|r_i\|}{\sum_{i=1}^{M} \|J_i\|^2} \|r_{test}\| \right|, \qquad (9)$$

4. Results:

4.1. Discrete Picard Plots

As a first step in solving the EEG inverse problem, the Discrete Picard Plots were obtained for the simulated EEG data sets corresponding to the dipole locations D1, D2, and D3. The simulated EEG data is obtained for the radial orientations of these test dipoles. A noise level of the signal to noise ratio (S NR) of 4 and 12 is added to the simulated EEG data. The Discrete Picard Plots describes the decaying rate of the absolute values of the SVD

coefficients (Fourier coefficients) and the decaying rate of the corresponding singular values in addition to the decaying rate of their ratio.

Authors found that the Discrete Picard Condition is satisfied for all datasets. It is clear from the plots that the rate of decay of the Fourier coefficients (black stars) is fairly faster than the decay rate of the singular values (blue dots) for small indexed singular values, as shown in figure 3. For higher singular values the decay rate of the singular values becomes faster. These singular values correspond to noise and must be truncated to obtain a useful solution. It is also clear in the figure that the rate of the decay of the Fourier coefficients increases as the SNR increase for the small indexed singular values as expected. Furthermore, Authors see that the location of the dipole does not affect the decay- ingrate of the singular values and the Fourier coefficients. However, authors must consider more locations to make such a conclusion. The satisfaction of the Picard condition indicates that it is possible to obtain a useful solution for the ill-posed problem.
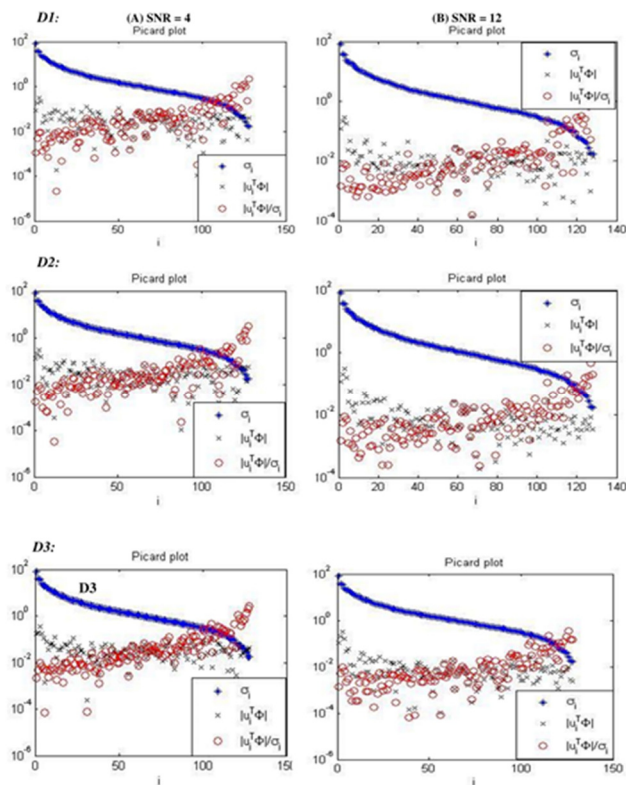

Figure 3. Discrete Picard Plots for the $D1$, $D2$, and $D3$ with radial orientation at different SNR (4 and 12). The blue dots are the singular values, the Fourier coefficients are shown in green and red circles are Fourier coefficients divided by singular values.

4.2 Estimation of α using NCP method, NCPs curves

Authors tuned the regularization parameter using the simulated EEG data sets corresponding to the three dipole locations with different orientations using L-curve, GCV, and NCP methods. Authors added different levels of noise to the simulated EEG data. In order to observe the effect of the white Gaussian noise, authors plotted the NCP of the simulated EEG data Φ corresponding to the dipole location $D1$ without noise and after adding white noise with $SNR = 6$. In figure 4, authors see that the noisy data set Φ (green line) fits within Kolmogorov-Smirnoff (KS) limits, which means that it is dominated by low-frequency components. The two gray lines in the figure correspond to the KS limits.

The NCPs curves for the three simulated EEG data sets corresponding to the dipoles ($D1$, $D2$, and $D3$) with radial orientation are shown in figure 5. As the figure shows, some curves have a high-frequency component, while others have low-frequency components. Curves above the blue line correspond to high-frequency components. While those below the blue line corresponds to low-frequency component. The blue line represents the optimal NCP, which corresponds to the optimal regularization parameter. On the other hand, for smaller $S NR = 4$, most of the NCP curves are below the blue line KS corresponds to low-frequency components. This means that these components have higher white noise compared to 16 SNR case as expected. Also, authors can see that for deep current sources in the brain ($D3$ and $D2$), the NCPs of the residual vector become closer to each other and they fit within KS limits. The difference can be noticed in the figure 5 part A.
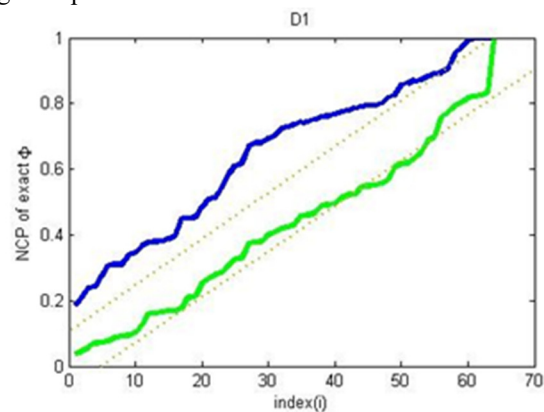

Figure 4: The NCPs for the synthetic exact (Blue line), and the NCP of the synthetic data after adding white Gaussian noise

4.3. Estimating the solution using WMNE algorithm

Here authors present the results obtained using WMNE algorithm (Hamalainen, 1984; Lin et al., 2006). Authors opted WMNE algorithm to solve the EEG inverse problem because it has no reference to the superficial dipoles as in the case of minimum norm estimate. Authors computed the weighting matrix as illustrated in the Pascual-Marqui, 2007 study, authors inserted the computed regularization parameter by the previous three illustrated methods into the algorithm. Figure 6 shows the results in

terms of three error measures, localization error, the center of gravity and spatial spreading, respectively.

Figure 6 shows the error measures obtained by using WMNE method in terms of SNR. For these solutions, the optimal regularization parameter α was obtained using the L-curve (green line), GCV (black line) and
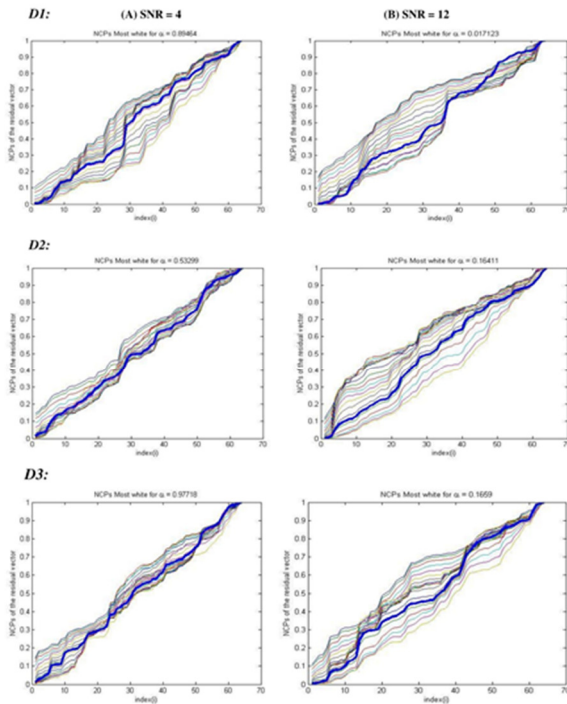
Figure 5. The NCPs curves for shallow $D1$, mid $D2$, deep $D3$ dipoles for two levels of signal to noise ratio (from left to right). The red thick line represents the optimum NCP, which corresponds to the optimum regularization parameter.

NCP (red line). The synthetic data sets used corresponds to three test dipole locations, the left subfigure of figure 6 corresponds to $D1$, middle sub figure corresponds to $D2$ and the right corresponds to $D3$.

It can be clearly seen that for the three dipole locations, the localization error is highest when WMNE method uses the regularization parameter obtained using the L- curve method compared to those obtained when using the NCP and GCV method. On the other hand, the localization error is small when WMNE algorithm uses the NCP methods compared to the error obtained when GCV method is used. For instance, at $S\ NR = 14$, the error was 22.3 mm when L-curve is used compared to 20.2 mm when GCV is used and 19.1 mm when NCP is used.

Furthermore, it is clear that the localization errors decrease with increasing the signal-to-noise ratio (SNR) when using the three methods for all dipole locations. These results agree with the intuition. Further, authors see that the localization error slightly increases at SNR values

of 2 to 4 as the depth of the test dipole location increases, but it does not change much at SNR =14.

These results indicate that the WMNE can overcome the bias toward superficial sources of the minimum norm estimate (*MNE*) method and the method can handle deep current source generators as well, and this came in agreement with the literature (Lin et al., 2006; Pascual-Marqui, 2002). These error results are the average of using 30 uniformly distributed orientations for each test dipole location. Figure 6 *B*), shows the errors measure defined as the distance of the location of the center of gravity of the estimated current to the actual dipole location (COG error). Using this measure, our results indicate similar to localization error measure performance result. It can be seen that when α, obtained using the L-curve method, used in the WMNE, the COG error is the high- est for the three dipole locations. In contrast, the accuracy obtained using the NCP and GCV methods are almost the same according to this measure. However, in some cases, the GCV method outperforms the NCP method. Furthermore, it is clear that the COG measure decreases with increasing the signal to noise ratio when using the three methods for all datasets corresponding to three dipole locations. According to this measure, a small increase in the errors is noticed when authors move from the superficial dipole to deep dipole locations, in particular when authors used low SNRs, such as 2 and 4. But, when SNR = 12, or 14, the positions of the dipole did not affect the COG error since they reach the same amount of errors.

The third measure authors considered is the spatial spreading, which provides a measure of how the solution is focused in space. A focused solution gives a distribution of the estimated current values such that it is high around the active region while it is low far away from the active region. It is desired to obtain a focused solution. According to the spatial spreading measure, our results shown in figure 6 C indicate that the solution obtained using the L-curve gives the least focused solution compared to the solution obtained using the NCP and GCV methods. Further, solutions obtained using the NCP are slightly more focused than the solution obtained using GCV method. And it is clear that the spatial spreading measure decrease with increasing the signal to noise ratio, which means larger noise produce blurred less focused solutions. Moreover, the focus of the solution remains the same as authors move to deeper locations.

5. Conclusion:

In this paper, authors show the results of using three regularization parameter choice methods (L-curve, Generalized cross-validation and normalized cumulative periodogram) for tuning the regularization parameter of EEG inverse problem of the source localization. Source Localization aims to find the sources of the neural activities inside the brain.
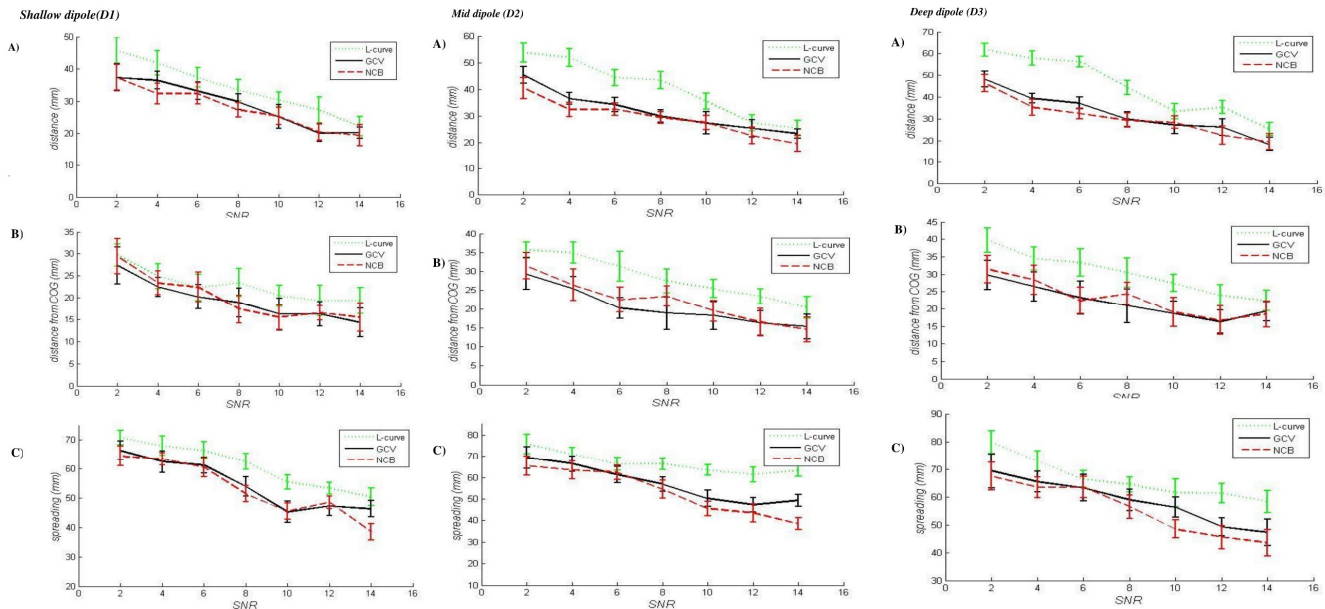
Figure 6. Using WMNE algorithm, for shallow dipole, dipole in the middle and deep located dipole, from left to right, A) The localization error (mm) in terms of SNR after obtaining from L-curve, GCV and NCP. B) Distance from the center of gravity (mm) in terms of SNR. C) Spatial spreading in terms of SNR.

The inverse ill-posed problem is characterized by a difficulty of tuning the regularization parameter of the Tikhonov regularization. Estimating the optimal or near optimal parameter improves the localization error in finding an estimated solution of the problem.

Distributed dipole model approach was used in this study for solving the source localization problem, authors used a computational human head model as a volume conductor consists of 5 different uniform tissues to solve the EEG forward problem, the forward problem was solved using the Alternating Direction Implicit (ADI) algorithm. Whereas, WMNE algorithm is used as a solver of the inverse problem.

Three dipole locations have been selected to generate the synthetic EEG data (shallow location, at the middle of the cortex and deeply located dipole) with different noise levels. The application of the L-curve and NCP methods requires the problem to satisfy the Pi- card Condition and the noise must be white Gaussian. In order to check the satisfaction of these conditions, authors checked the Picard condition for the three dipole locations with two signals to noise ratios.

The L-curve, GCV curve and the NCPs curve have been plotted. The plots correspond to the three test dipole locations. The next step was to tune the regularization parameter using the three-parameter choice methods (L-curve, GCV, and NCP), authors inserted these parameters into the WMNE algorithm to solve the inverse problem. Authors evaluated the WMNE solution using three measures (Localization error, the center of gravity and spatial spreading). For the three measures, the algorithm gives the highest errors when it uses α obtained using L-

curve, then *GCV* and *NCP*, respectively. Although, the algorithm with α obtained using GCV method sometimes gives error values similar to those obtained using the NCP method. Also, WMNE handled the three locations without any bias, since it gives similar localization error at the three dipole locations.

Corresponding Author:
Mohammed Aburidi, Ph.D.
Computer Science Department, An-Najah National University, Nablus, Palestine.
E-mail: mohammed.ridi114@gmail.com

References:
1. Baillet, S. (1998). Toward functional brain imaging of cortical electrophysiology Markovian models for magneto and electroencephalogram source estimation and experimental assessments. *Orsay, France*, *11*.
2. Baillet, S., Mosher, J. C., & Leahy, R. M. (2001). Electromagnetic brain mapping. *IEEE Signal processing magazine*, *18*(6), 14-30.
3. Baillet, S., Riera, J. J., Marin, G., Mangin, J. F., Aubert, J., & Garnero, L. (2001). Evaluation of inverse methods and head models for EEG source localization using a human skull phantom. *Physics in medicine and biology*, *46*(1), 77.
4. Cherry, S. R., & Phelps, M. E. (1996). Imaging Brain Function with Positron Emission Tomography-18.
5. Clerc, M., Adde, G., Kybic, J., Papadopoulo, T., & Badier, J. M. (2005). In vivo conductivity estimation with symmetric boundary elements. *International Journal of Bioelectromagnetism*, *7*, 307-310.

6. Darvas, F., Pantazis, D., Kucukaltun-Yildirim, E., & Leahy, R. M. (2004). Mapping human brain function with MEG and EEG: methods and validation. *NeuroImage*, *23*, S289-S299.

7. De Munck, J. C. (1988). The potential distribution in a layered anisotropic spheroidal volume conductor. *Journal of applied Physics*, *64*(2), 464-470.

8. Fender, D. H. (1987). Source localization of brain electrical activity. *Handbook of electroencephalography and clinical neurophysiology*, 355-403.

9. Golub, G. H., Heath, M., & Wahba, G. (1979). Generalized cross-validation as a method for choosing a good ridge parameter. *Technometrics*, *21*(2), 215-223.

10. Gonçalves, S. I., de Munck, J. C., Verbunt, J. P., Bijma, F., Heethaar, R. M., & da Silva, F. L. (2003). In vivo measurement of the brain and skull resistivities using an EIT-based method and realistic models for the head. *IEEE Transactions on Biomedical Engineering*, *50*(6), 754-767.

11. Grech, R., Cassar, T., Muscat, J., Camilleri, K. P., Fabri, S. G., Zervakis, M., ... & Vanrumste, B. (2008). Review on solving the inverse problem in EEG source analysis. *Journal of neuroengineering and rehabilitation*, *5*(1), 25.

12. Greenblatt, R. E., Ossadtchi, A., & Pflieger, M. E. (2005). Local linear estimators for the bioelectromagnetic inverse problem. *IEEE transactions on signal processing*, *53*(9), 3403-3412.

13. Hallez, H., Vanrumste, B., Van Hese, P., D'Asseler, Y., Lemahieu, I., & Van de Walle, R. (2005). A finite difference method with reciprocity used to incorporate anisotropy in electroencephalogram dipole source localization. *Physics in medicine and biology*, *50*(16), 3787.

14. Hamalainen, M. S. (1984). Interpreting measured magnetic fields of the brain: estimates of current distributions. *Helsinki Univ. of Technol., Rep.*

15. Hämäläinen, M., Hari, R., Ilmoniemi, R. J., Knuutila, J., & Lounasmaa, O. V. (1993). Magnetoencephalography—theory, instrumentation, and applications to noninvasive studies of the working human brain. *Reviews of modern Physics*, 65(2), 413.

16. Hansen, P. C. (1994). Regularization tools: A Matlab package for analysis and solution of discrete ill-posed problems. *Numerical algorithms*, *6*(1), 1-35.

17. Hansen, P. C. (2001). The L-curve and its use in the numerical treatment of inverse problems, Computational Inverse Problems in Electrocardiology, Advances in Computational Bioengineering Series, vol. 4. *WIT Press, Southampton*, *159*, 119-142.

18. Hansen, P. C., & Kilmer, M. E. (2007). A parameter‐choice method that exploits residual information. *PAMM*, 7(1), 1021705-1021706.

19. Hansen, P. C., & O'Leary, D. P. (1993). The use of the L-curve in the regularization of discrete ill-posed problems. *SIAM Journal on Scientific Computing*, *14*(6), 1487-1503.

20. Hansen, P. C., Kilmer, M. E., & Kjeldsen, R. H. (2006). Exploiting residual information in the parameter choice for discrete ill-posed problems. *BIT Numerical Mathematics*, *46*(1), 41-59.

21. Krawczyk-StańDo, D., & Rudnicki, M. (2007). *Regularization* parameter selection in discrete ill-posed problems—the use of the U-curve. *International Journal of Applied Mathematics and Computer Science*, *17*(2), 157-164.

22. Lin, F. H., Witzel, T., Ahlfors, S. P., Stufflebeam, S. M., Belliveau, J. W., & Hämäläinen, M. S. (2006). Assessing and improving the spatial accuracy in MEG source localization by depth-weighted minimum-norm estimates. *Neuroimage*, *31*(1), 160-171.

23. Liu, A. K., Belliveau, J. W., & Dale, A. M. (1998). Spatiotemporal imaging of human brain activity using functional MRI constrained magnetoencephalography data: Monte Carlo simulations. *Proceedings of the National Academy of Sciences*, *95*(15), 8945-8950.

24. Meijs, J. W. H., ten Voorde, B. J., Peters, M. J., Stok, C. J., & Lopes da Silva, F. H. (1988). *The influence of various head models on EEGs and MEGs* (pp. 31-45). Berlin, Germany: Springer-Verlag.

25. Modarreszadeh, M., & Schmidt, R. N. (1997). Wireless, 32-channel, EEG and epilepsy monitoring system. In *Engineering in Medicine and Biology Society, 1997. Proceedings of the 19th Annual International Conference of the IEEE* (Vol. 3, pp. 1157-1160). IEEE.

26. Morozov, V. A. (1966). On the solution of functional equations by the method of regularization. In *Soviet Math. Dokl*. 7(1), 414-417.

27. Munck, D. J., & Peters, M. J. (1993). A fast method to compute the potential in the multisphere model. *IEEE transactions on biomedical engineering*, *40*(11), 1166-1174.

28. Neilson, L. A., Kovalyov, M., & Koles, Z. J. (2005). A computationally efficient method for accurately solving the EEG forward problem in a finely discretized head model. *Clinical neurophysiology*, *116*(10), 2302-2314.

29. Oostendorp, T. F., Delbeke, J., & Stegeman, D. F. (2000). The conductivity of the human skull: results of in vivo and in vitro measurements. *IEEE transactions on biomedical engineering*, *47*(11), 1487-1492.

30. Pascual-Marqui, R. D. (1999). Review of methods for solving the EEG inverse problem. *International journal of bioelectromagnetism*, *1*(1), 75-86..

31. Pascual-Marqui, R. D. (1999). Review of methods for solving the EEG inverse problem. *International journal of bioelectromagnetism*, *1*(1), 75-86.

32. Pascual-Marqui, R. D. (1999). Review of methods for solving the EEG inverse problem. *International journal of bioelectromagnetism*, *1*(1), 75-86.

33. Pascual-Marqui, R. D. (2002). Standardized low-resolution brain electromagnetic tomography (sLORETA): technical details. *Methods Find Exp Clin Pharmacol*, *24*(Suppl D), 5-12.

34. Pascual-Marqui, R. D. (2002). Standardized low-resolution brain electromagnetic tomography (sLORETA): technical details. Methods Find Exp Clin Pharmacol, 24(Suppl D), 5-12.

35. Pascual-Marqui, R. D. (2007). Discrete, 3D distributed, linear imaging methods of electric neuronal activity. Part 1: exact, zero error localization. *arXiv preprint arXiv:0710.3341*.

36. Pascual-Marqui, R. D., Lehmann, D., Koenig, T., *Kochi*, K., Merlo, M. C., Hell, D., & Koukkou, M. (1999). Low resolution brain electromagnetic tomography (LORETA) functional imaging in acute, neuroleptic-naive, first-episode, productive schizophrenia. *Psychiatry Research: Neuroimaging*, *90*(3), 169-179.

37. Rubio, D., & Troparevsky, M. I. (2006). The EEG forward problem: theoretical and numerical aspects. *Latin American applied research*, *36*(2), 87-92.

38. Salman, A., Malony, A., Turovets, S., Volkov, V., Ozog, D., & Tucker, D. (2013). Next-generation human brain neuroimaging and the role of high-performance computing. In *High Performance Computing and Simulation (HPCS), 2013 International Conference on* (pp. 234-242). IEEE.

39. Scherg, M., & Von Cramon, D. (1985). Two bilateral sources of the late AEP as identified by a spatio-temporal dipole model. Electroencephalography *and Clinical Neurophysiology/Evoked Potentials Section*, *62*(1), 32-44.

40. Tong, S., & Thakor, N. V. (2009). *Quantitative EEG analysis methods and clinical applications*. Artech House.

41. Tucker, D. M. (1993). Spatial sampling of head electrical fields: the geodesic sensor net. *Electroencephalography and clinical neurophysiology*, *87*(3), 154-163.

42. Van Uitert, R., & Johnson, C. (2002). Can a spherical model substitute for a realistic head model in forward and inverse MEG simulations?. In *Proceedings of BIOMAG*. 25, 52-68.

43. Van Uitert, R., Weinstein, D., & Johnson, C. (2003). Volume currents in forward and inverse magnetoencephalographic simulations using realistic head models. *Annals of Biomedical Engineering*, *31*(1), 21-31.

44. Wahba, G. (1977). Practical approximate solutions to linear operator equations when the data are noisy. *SIAM Journal on Numerical Analysis*, *14*(4), 651-667.